
Article:
Oseghale, C.I., Abdalla, A.H., Posada, J.O.G. et al. (1 more author) (2016) A new synthesis route for sustainable gold copper utilization in direct formic acid fuel cells. International Journal of Hydrogen Energy, 41 (37). pp. 16394-16401. ISSN 0360-3199

https://doi.org/10.1016/j.ijhydene.2016.05.204

A new synthesis route for sustainable gold copper utilization in direct formic acid fuel cells

C.I. Oseghale[1], A. H. Abdalla, J. O. G. Posada and P.J. Hall
Department of Chemical & Biological Engineering, University of Sheffield, Mappin Street, Sheffield, S1 3JD, England, UK; charles.oseghale@sheffield.ac.uk

Abstract

In the efforts to develop a more sustainable energy mix there is an urgent need to develop new materials for environmentally friendly processes. Developing low metal loading anode catalyst with high electrocatalytic activity for liquid fuel cells remains a great challenge. Polyvinylpyrrolodone-protected AuCu-C core-shell was fabricated by a facile one-pot modified chemical reduction method. The nanoparticles were characterized by X-ray diffraction (XRD), transmission electron microscopy (TEM), scanning electron microscopy (SEM), energy dispersive X-ray spectroscopy (EDS), and atomic force microscopy (AFM) analyses. XRD analysis indicates the preferential orientation of catalytically active (111) planes in AuCu-C core-shell nanoparticles. The inclusion of Cu in the AuCu-C catalysts increased catalytic activities, which can be attributed to the increases lattice parameters. Comparative results show that AuCu-C catalyst exhibited much better electrocatalytic activity and stabilization compared to commercial Au nanoparticle on carbon support catalyst. The high performance of AuCu-C catalyst may be attributed to the electronic coupling or synergistic interaction between Cu core structure, and the Au shell makes it a promising for DFAFCs applications.

Keywords: Synthesis, Core-Shell, Catalyst, low-cost, DFAFCs

1 Introduction

The growing demand of energy from renewable sources has seen rapid increase in research and development of new technology [1]. There is global concern to develop technologies that can improve the reliability, efficiency and quality of energy supply. Intermittent renewable energy sources are an immediate form of energy that must be used as available or converted into a different form for storage, otherwise they will be lost. Fuel cells (FCs) have great potential to backup renewable energy sources owing to the intermittent weather conditions [2-4], which causes problems in the control of load frequency, generator voltage and system stability [5]. However, development of fuel cells still face challenges in the area of research and development of membranes, new efficient and inexpensive electrode materials (anode catalysts), and current collectors to effectively harness/balance the performance-cost inequalities for commercialization of these technologies [6-8]. Global demand for commercial fuel cell products due to technological advancement, improved manufacturing and government policies is forecasted to triple from $4 billion in 2017 to as high $12 billion by 2022 [9].

Direct formic acid fuel cells (DFAFCs) are a viable solution for overcoming the irregularity of power supply. Also DFAFCs have the potential to reduce carbon emission from the current electricity network. In addition, this technology exhibits high efficiency, low operating temperature and fast-start-up for portable applications [10].

[1] Corresponding author. Chemical and Biological Engineering, University of Sheffield, Sir Robert Hadfield Building, Mappin Street, Sheffield S1 3JD, England, UK. Tel: +44(0)1142227555. Fax: +44(0)1142227501. E-mail: charles.oseghale@sheffield.ac.uk

Dilute formic acid, as a liquid and strong electrolyte is non-toxic, non-corrosive and non-flammable, which are attractive features when compared with current the challenges of hydrogen gas storage [3, 11-13]. Formic acid (FA) as hydrogen-storage material can release hydrogen at ambient temperature compared to methanol, ethanol, metal hydrides which require high temperature and pretreatment to avoid CO poisoning [14-18]. For example, different supported catalysts have been demonstrated to release CO-free H_2 from HCOOH, Au-ZrO_2 [19], Pd/C [20] at temperature range of 21 to 60 ^{o}C. Formic acid has a high energy-conversion efficiency as a liquid fuel is easy to deliver with current pipe networks, transportation systems and excellent storage potential [21].

Electrooxidation of FA is thought to proceed via two parallel pathways, which require suitable catalysts compared with the direct reaction route. The direct pathway (Equation 1), FA is directly oxidized to CO_2 without formation of a CO intermediate. The second route is the "CO pathway"; FA reacts to form CO intermediate, and is then oxidized to CO_2 (Equation 2) [16, 22-25]. This CO poisoning pathway may be avoided by adjusting the reaction conditions such as reaction temperature, pH of the electrolyte and choice of catalyst type [26].

$$HCOOH \rightarrow CO_2 + 2H^+ + 2e^- \qquad \Delta G_{298\,K} = -35.0 \text{ KJ mole}^{-1} \qquad (1)$$

$$HCOOH \rightarrow CO_{abs} + H_2O \rightarrow CO_2 + 2H^+ + 2e^- \qquad \Delta G_{298\,K} = -14.9 \text{ KJ mole}^{-1} \qquad (2)$$

One problem inhibiting the commercialisation of fuel cells is the cost, selectivity and stability of the catalyst. Platinum (Pt) and Pt-group metals have been extensively studied due to their high reactivity. However, Pt catalysts have limitations such nanoparticle aggregation under operating conditions, CO deactivation of active sites, scarcity and high cost for large scale application [27]. Therefore, design and synthesis of new anode catalysts with reduced metal loading and high catalytic activity is highly desirable but challenging.

Compared with Pt, gold is relatively abundant and has a high oxidation activity for small organic molecules due to its high resistance against surface oxides [28-30]. Small gold nanoparticles have demonstrated unusual optical properties, size-dependent electrochemistry and have become the model of choice for self-assembly, drug delivery, biolabeling, catalysis, and crystal growth [31, 32]. Supported gold nanoparticles have proven to be extremely active catalysts in oxidation of various small organic compounds [33]. Bimetallic catalysts have shown to have remarkable ability to enhance reactivity, selectivity and stability of oxidative processes [1, 17, 34-38]. The superior performance of bimetallic structures in comparison with monometallic particles is due to the synergistic effect of the admetals. A core-shell structure is one solution to reducing anode catalyst cost, improving utilization. and enhancing the performance of DFAFCs electrooxidation processes. Core-shell bimetallic, unlike alloyed catalysts do not exhibit poor long-term stability because of dissolution of non-noble metals [39]. Recent research have shown that controlled synthesis strategy for preparing nanocatalysts produce well-defined and durable surface structures [40]. Nanostructuring of gold-copper catalysts provide an effective design to improve the utilization of expensive and highly active noble metals as a metal shell (gold) on a copper (core) [41]. Hsu and co-workers recently reported the effect of electronic coupling in optimization and tailoring of Au/Pd core-shell catalyst with superior electrochemical stability in comparison with commercial catalysts [42]. There are varieties of reasons for the synergistic effect of bimetallic catalysts such as possible combinations of reactants, compositions and experimental conditions, which often are not fully characterized, limiting direct correlation between bimetallic systems and catalytic properties [43]. Ren and co-workers confirmed that the copper content within catalysts increase lattice strain in nanocrystals, thus leading to downshift of the d-band centre with overall improved catalytic performance [44].

In this article, we present a state-of-the-art formic acid fuel cell electrocatalyst comprising a gold shell and copper core on carbon black support. In order to achieve a controlled core shell structure and

reveal the real electrochemical properties of AuCu on carbon black support, we employed a two-stage synthesis route at low temperature. Copper precursor stabilize with polyvinylpyrrolodone (PVP) reduced with sodium borohydride form Cu-PVP stabilize nanoparticles for gold layer deposition. High concentration of sodium hydroxide added decrease of water molecules available for hydrolysis reaction of sodium borohydride. This suppressed the hydrogen evolution and generation of zero valent Cu and Au nanoparticles. This is a facile and scalable approach to prepare AuCu-C core shell bimetallic catalysts. Compared with monometallic Au nanoparticles with same metal loading, AuCu-C catalyst synthesized in this work demonstrated remarkable electrocatalytic activity for formic acid oxidation at room temperature. Detailed physical and electrochemical measurements were performed to correlate AuCu-C bimetallic structure and catalytic properties and compared with commercial gold nanoparticles dispersed on carbon black.

2 Experiment and methods

2.1 Synthesis of AuCu-C catalysts

AuCu-C catalysts were prepared by measuring, 140 mg of polyvinylpyrrolodone (PVP, 1.30 mmol of monomeric units, Mw = 40,000, 99.9% Sigma-Aldrich), 10 mL of fresh deionized water (18.2 $M\Omega.cm^{-1}$, Purelab option ELGA) and 1.1 mL of 0.062 mol/L copper sulphate ($CuSO_4.5H_2O$ in H_2O, 99.99%, Aldrich). The obtained solution was purged with argon gas for approximately 1h in order to remove dissolved O_2. Then a freshly prepared 10 mL of 1M solution of sodium borohydride ($NaBH_4$, 99%, Aldrich) was added dropwise to the $CuSO_4$-PVP solution with continuous stirring and protected with argon gas. The temperature of the solution was then raised to about 50 ^oC and the reaction was allowed to proceed for 1h to yield Cu nanoparticles. Deaerated freshly prepared 0.35 mL of (0.05 mol/L) $HAuCl_4.3H_2O$ solution (99.9% Sigma-Aldrich) was quickly added to the $CuSO_4$-PVP nanoparticle solution and stirred for 1h under argon protection. The redox potential of Au^{3+}/Au is higher than that of Cu^{2+}/Cu, Au (III) is reduced to Au and therefore Cu-Au particles were formed (see figure 1). Within a few minutes of sol generation, the sol is immobilized by adding KetJenblack (ECP600JD) under vigorous stirring for 30 min and then allowed to settle for 30 min. The amount of support is calculated as having a final Au-Cu loading of 20 wt.%. The resulting Carbon black-supported AuCu catalysts were obtained by filtering the resultant solution using a Whatman cellulose nitrate filter paper. The AuCu-C catalysts were washed several times with deionized water to remove any free PVP macromolecules not bound to AuCu-C catalysts and until no chloride ion (Cl^-) was detected in the washing solution. The Au-Cu-C catalysts were dried under vacuum at 80^oC overnight to obtain the final catalysts.

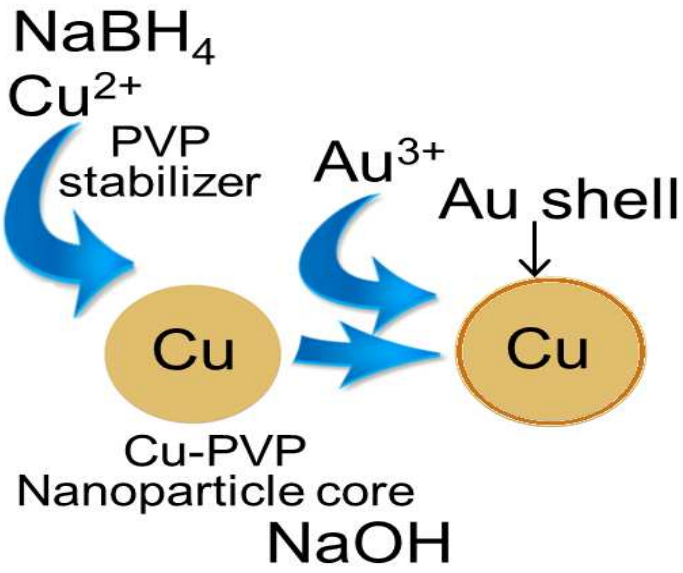

Figure 1. Schematic illustration of the formation of AuCu-C core-shell nanoparticles

2.2 Cyclic Voltammetry (CV) Experiment

CV experiments were performed in 0.5 M H_2SO_4, (95-97%, Aldrich) in the potential range of -0.2 to 1.0 V (Ag/AgCl, KCl_{std}) at a scan rate of 20 mVs^{-1}, and in 0.5M HCOOH + 0.5M H_2SO_4 in the potential range of -0.4 – 1.6V (Ag/AgCl, KCl_{std}) at a scan rate of 2 mVs^{-1}. The working electrode was polished to a mirror finish using 0.5 and 0.05μm alumina suspensions sequentially before use. Appropriate dilution ratio of catalysts, analytical grade ethanol (96%, Aldrich) and 5wt% Nafion solution (99.99%, Aldrich) were mixed for 1h. On the surface of the GCE (OD: 6 mm ID: 3.0 mm), 9μL slurry was spread and dried overnight at 80 ^oC to obtain the working electrodes. The apparent surface area of glassy carbon electrode was 0.07cm^2. The gold nanoparticles-5 nm diameter, OD 1, stabilized suspension in citrate buffer (Sigma-Aldrich) was dispersed in ethanol and carbon black. The 20wt% AuCu loading of the electrode was 0.31 mg/cm^2.

2.3 Physical Characterisation of Catalysts

Samples were prepared for imaging by deposition of AuCu-C catalyst slurry dispersed in ethanol and ethylamine solution on a freshly cleaved mica surface. The freshly cleaved circular mica sheets glued to a metal pad were used for sample analysis on the AFM imaging. After deposition, samples were allowed to dry in air and then transferred for AFM imaging. AFM imaging was performed on the Dimension icon with ScanAsyst system (Bruker Ltd, Germany) operating in soft tapping mode in air at room temperature. All cantilevers used throughout the experiments were silicon reflective aluminium coating with 3.7 μm thickness. According to producer's specifications, spring constant was 26 N/m, resonance frequency of 300 kHz and radius tip was 7 nm. All images were flattened, and then used section analysis and particle size determination. X-ray diffractometer (model D2 Phaser Bruker Ltd) was employed for the phase identification with CuKα1 radiation (λ = 1.5406 Armstrong) and a graphite monochromator were maintained at a tube voltage and current of 30 kV, 10 mA, respectively to obtain X-ray diffraction (XRD) patterns of the sample. The 2θ angular region between 10^o – 90^o were explored at a scan rate (1^o min^{-1}), with a step size of 0.1 and increment (i.e. step size between data point) of 0.02. The primary divergence slit of 0.6 mm was used and Ni K-beta filter was not fitted because of the carbon black support. The structure and morphology of the catalyst were examined by a FEI Tacnai 20 transmission electron microscope (TEM) at 200 kV. Samples were prepared by adding about ~1mg/ml of the nanoparticle dispersed in 96% ethanol solution onto a 200-mesh copper grid and drying in air to room temperature. Scanning electron microscopy (SEM) images were recorded using Jeol JSM-6010LA analytical scanning electron microscope at 20 kV. All samples were prepared by dispersing 1 mg of Pd-C catalysts in 1 mL of 96% ethanol and sonicated for 1 minute in water bath. 10 μL of the paste was cast on Jeol 10 mm x 10 mm diameter plain stubs and dried at room temperature.

3 Results and discussions

3.1 Crystallography of AuCu-C and Au-C catalysts

The crystal phases of the AuCu-C catalysts were characterised using XRD. The diffraction peaks match very well with the tetragonal face-centred cubic Au crystalline structure (JCPDS 4-0784). Compared with the reflection Au-C catalysts, the diffraction planes of AuCu-C catalysts shifted to higher due to the presence of the Cu contents. For example, the Au-C (200) at 44.19° shifted to lower 44.09° because of the lattice contraction between metals with different lattice spacing, indicating the reason for the marked decrease in the mean d-spacing [44].

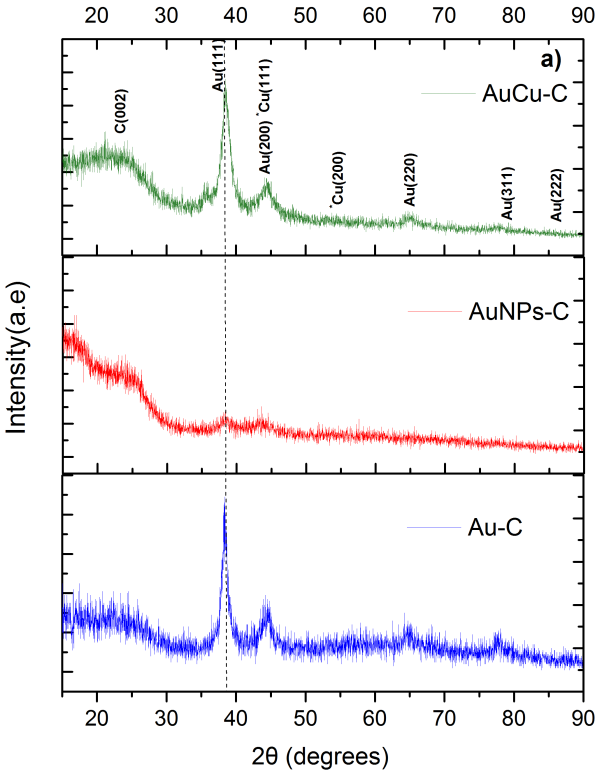

Figure. 2. The XRD patterns of Au-C, AuCu-C and AuNPs-C.

This shows the complete coverage of the copper (core) nanoparticle by gold (shell). AuCu nanoparticles will show reflections according to the selection rules for crystal diffraction, where the Miller indices (*hkl*) are all odd or all even Au (111), Au (200), Au (220), Au (311), and Au (222), respectively. The absence of the superlattice reflections of 001 and 110, and the splitting reflections of 200/002 and 220/202 indicated the formation of core-shell structure instead of ordered intermetallic structure of an alloy [34, 40, 45]. AuCu exhibited a shift from pure Au nanoparticles (2θ = 38.3, 44.4, 64.6 and 77.7) indicative of the absence of alloy structure formation. Table 1 presents the particle size analysis of AuCu and Au catalysts on carbon support. The mean particle size (*d*), were calculated from the X diffraction plane using Debye-Scherrer's equation (equation 3)[30, 46].

$$d = \frac{0.94\lambda}{\beta \cos\theta} \tag{3}$$

where, d is the average particle size, nm, λ is the x-ray wavelength (1.54056 Å for Cu K_α radiation), β is the full width at half-maximum in radians (FWHM) and θ is the angle of Au (111) peak. The peak width β and peak position θ were obtained from curve fitting using PANalytical Data Viewer software. There were no impurity phases detected, indicating the formation of pure and highly crystalline AuCu nanoparticles.

The relative crystallinities of Au nanoparticles are the ratio of the intensities of Au (111) and carbon peaks are 6.64 for AuCu-C and 2.47 for Au-C catalysts, respectively. This indicates a well crystalline Au and AuCu nanoparticles on carbon support. It is observed that a higher *d* space (d_{111} = 2.3234 Å) could be due to the lower 2θ peak of (111) of Au (d_{111} = 2.3503 Å) because of the incorporation of Cu atoms, indicating that core shell structure on carbon supported [47]. Neither metallic Cu nor Cu oxides reflections were detected in AuCu-C catalyst, suggesting that Cu exist as highly dispersed core species as shown in similar work by Duan and co-workers [39]. Similar behaviour of the absence of CuO

phase was also observed in [33]. Compared with pure Au pattern, AuCu-C slightly shifted to lower angles confirming core shell architecture. For example, AuCu did not match the AuCu alloy (JCPDS 1-072-5241) or $Cu_{0.508}$ $Au_{0.492}$ (JCPDS 4-018-5478) shifted to lower angles due to Cu content. This lattice contraction is due to the different in lattice spacing between two metals in solution is ascribed to Vegard's law [44]. Furthermore, individual Au and Cu nanoparticles formation can be ruled out, as the x-ray scattering of the physical mixtures would exhibit completely different XRD patterns.

In order to determine the Au crystallite structure from the XRD analysis and understand the effect of preferential orientation of crystal planes, the texture coefficient was determined. The texture coefficient measures the relative degree of preferred orientations among crystal planes. The texture coefficient was calculated using Halls method for each crystal plane of the XRD powder pattern of Au-C and AuCu-C catalysts, using equation (4) [48]:

$$TC_{(hkl)} = \frac{I_{(hkl)_i}/I_{o}I_{(hkl)_i}}{\frac{1}{n}\sum n\frac{I_{(hkl)_n}}{I_{o}I_{(hkl)_n}}} \quad (4)$$

where $TC_{(hkl)}$ is the texture coefficient of the facet (*hkl)*, $I_{(hkl)}$ is the intensity of the (*hkl*) reflection of the samples, $I_{o(hkl)}$ is the intensity of the (*hkl*) reflection of a polycrystalline bulk sample (Au bulk) and 'n' is the number of reflections taken into account. The texture coefficient general is expected to be unity for a facet with no preferential orientation. Above unity, the crystal planes are preferentially grown with respect to facets. The bulk gold face-centred cubic (fcc) structure matching (JCPDS, File No. 4-0784) was used for calculating the average crystallite size and texture coefficient of the different facets of the Au-C and AuCu-C catalyst particles (see Figure 3). The XRD data confirms that the Au and AuCu largely grows preferentially in the (111) orientation. The difference in crystallite size and texture between (111) and (200) even though parallel planes, imply that texture coefficient varies between polycrystalline and bulk sample and nanoparticles. The average crystallite size estimated from XRD is less than that from TEM, indicating the polycrystalline nature of the AuCu-C catalysts.

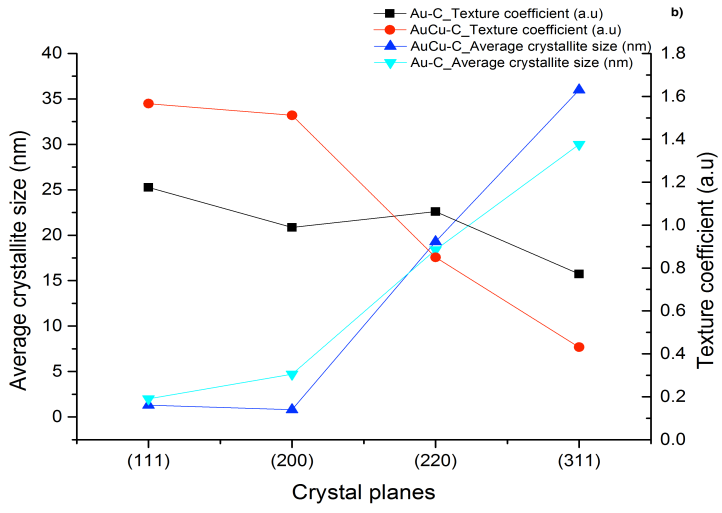

Figure.3. Texture coefficient and average crystallite size of Au-C and AuCu-C catalysts from XRD patterns

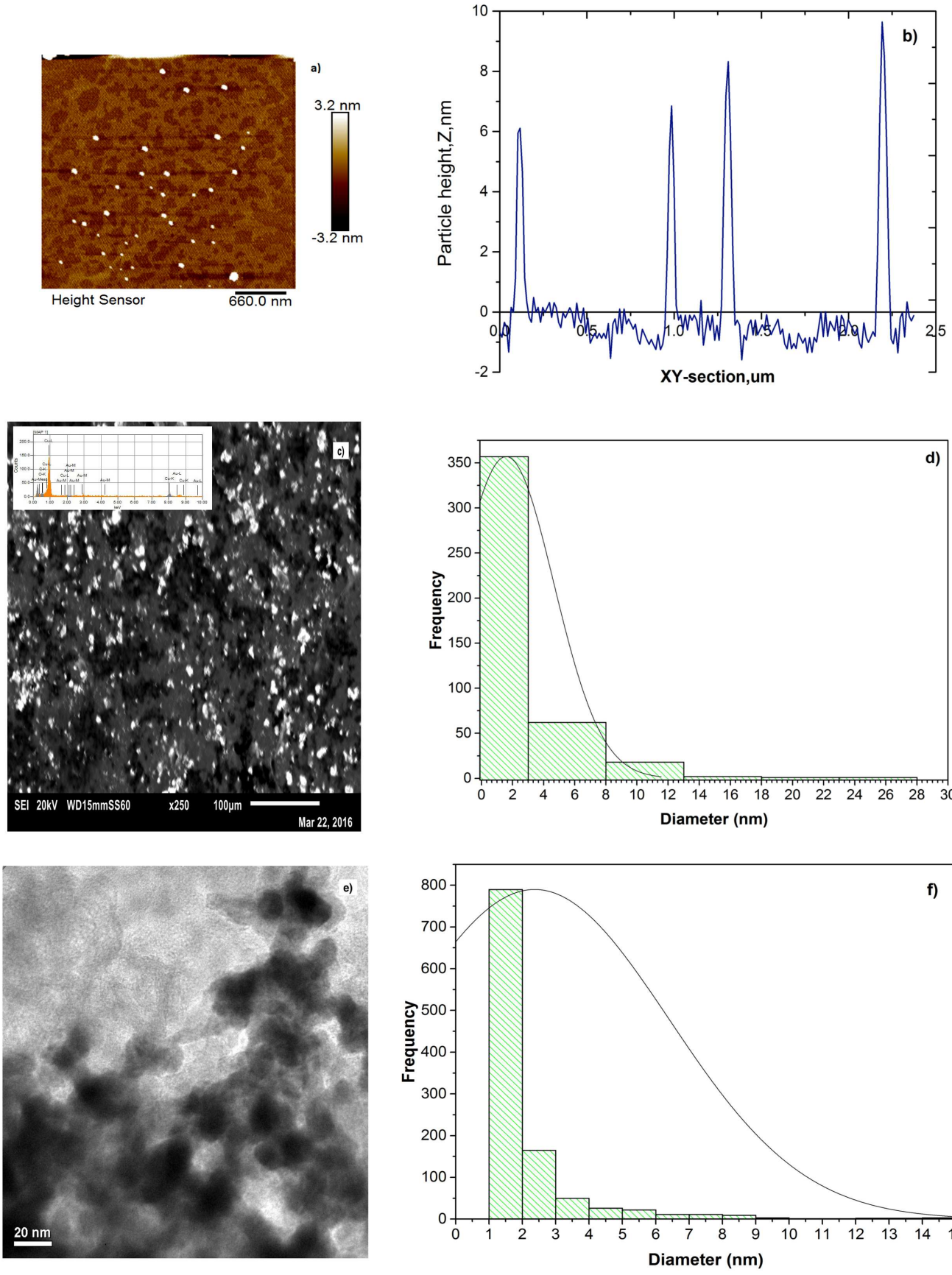

Figure 4. Morphology of AuCu-C catalyst: a) AFM image, b) AFM section analysis, c) SEM image with elemental mapping (inset), d) SEM particle distribution, e) TEM image, and f) TEM particle size histogram

3.2 Surface Morphology and Structure

The morphology and structure of the catalysts was studied using transmission electron microscopy (TEM), atomic force microscopy (AFM) and scanning electron microscopy (SEM). As shown in Figure 4, it can be observed clearly that the Au nanoparticles are well dispersed on the carbon support with a particle size in the region of 1-36 nm. From the histograms and section analysis, we can see few agglomerations, but core-shell structure also unfolded. The EDS results may suggest the formation of AuCu-C core shell, which is in fairly good agreement with the XRD core shell structure evaluation. Figure 4a shows the surface morphology of the AuCu-C catalyst deposited on mica sheet. The cross section analysis of image (Figure 4b) indicates showing the height of carbon black and the peaks of AuCu nanoparticles arising from the surface. The average particles size of 8.5 ± 0.56 nm is larger because of its convolution with tip width in measurement limiting high-resolution investigation [49, 50]. The peaks observed from the section analysis show AuCu nanoparticles anchored on carbon black of height between 1-14 nm. Figures 4c and 4d shows SEM microgram and histogram well displaying relatively well AuCu-C catalysts with nanoparticles with mean diameter distribution of 3.5 ± 0.31 nm, along with few agglomerate particles observed. The EDS elemental mapping confirmed the presence of Au and Cu dispersed on carbon support. The TEM image and analysis (figure 4e, 4f) illustrate from approximately 1120 particles, indicating more than 90% of average particles 1.4 ± 0.11 nm was in the observed range of 1 to 10 nm, which is in good agreement with XRD, AFM and SEM analysis results. These confirm that the TEM particle sizes represent a few single crystals AuCu or grains.

3.3 Electrocatalytic performance of AuCu-C for formic acid oxidation

Figure 5 shows the electrooxidation activity of formic acid on AuCu-C and AuNPs-C catalyst in the positive oxidation scan direction. From the profile of HCOOH oxidation, the main oxidation peaks are located at 1.36 V and 1.41 V, and current density of 13.2 and 4.2 mA cm^{-2}, respectively. The catalytic activity might be a result of the electronic structure as Au loses valence electrons to Cu and this perturbation positively affecting surface energy of Au to achieve improved electrochemical performance [44, 51]. This lead to weakness of the adsorption bonding energy of poisonous species during formic acid oxidation, indicating easy removal on catalyst active site [44], as observed with lower reversed onset potential 0.9 V.

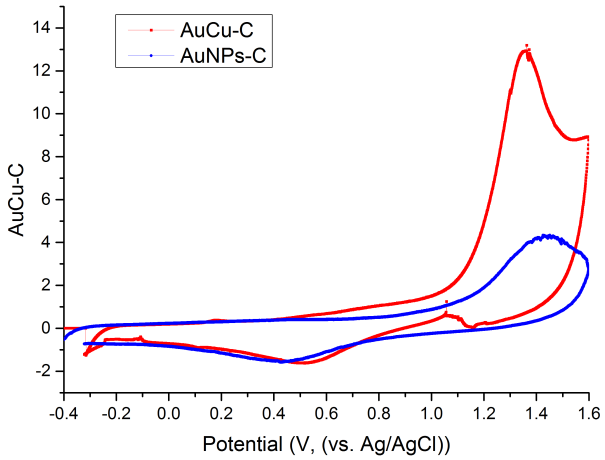

Fig.5. Cyclic Voltammogram at scan rate of 2mV/s, 25 ^{o}C.

Figure 5 demonstrates that the catalytic activity of AuCu-C is 3.14 time higher than commercial AuNPs dispersed on carbon black. It is proposed this enhanced catalytic activity is due to the synergistic effect of Cu in the AuCu-C catalysts [33, 44, 51], catalyst preparation, particle size, carbon

support, and reaction conditions. The performance is clearly dependent on lattice contraction associated with electronic effect and formation of core shell structure increasing coordination unsaturated Au and Cu for small molecule hydrocarbons. For example, experimental and computational estimates show that the bond dissociation energy values of Cu, Ag and Au are relatively high and also thermodynamically stable [52]. Another key influential factor for the high catalytic activity of AuCu-C is the adsorption of PVP on the surface of the nanoparticles preventing agglomeration and growth of nanoparticles as confirmed by Wang and co-workers [53]. It is observed that the lower onset potential for formic acid electrooxidation above, confirmed AuCu-C catalyst has better electrocatalytic activity.

Table 1 Physicochemical property of catalysts

Catalysts	d_{TEM}, Particle size (nm)	Chemical Surface Area (m^2/g)	Specific Activity (mA/m^2)	Mass Activity (m^2/g)	Roughness factor, R_f *E+6
AuNPs-C	1.4	62.1	0.003	0.7	8.87
AuCu-C	5.0	221.8	0.06	42.6	31.7
Au-C	1.2	258.8	0.016	13.5	37.0

Chronoamperometry is an effective method for evaluating the electrooxidation activities of the catalysts stability in acid medium. Figure 6 shows the chronoamperometry response of 0.5 M H_2SO_4 + 0.5 M HCOOH at a potential of 0.6 V versus Ag/AgCl sat KCl for 5000 seconds. All electrode catalysts showed current density decay for formic acid oxidation. The decay was faster in AuNPs-C electrodes than AuCu-C. The initial and final current density after 5000 seconds for AuNPs-C and AuCu-C were 11.4, 0.01 and 111.6, 0.005 mA cm^{-2}, respectively. As shown in table 1, that AuCu-C exhibited the largest mass activity under the employed condition, which confirms the very high electrocatalytic activity. This result is consistent with the physical characterizations from TEM, XRD and CV measurements.

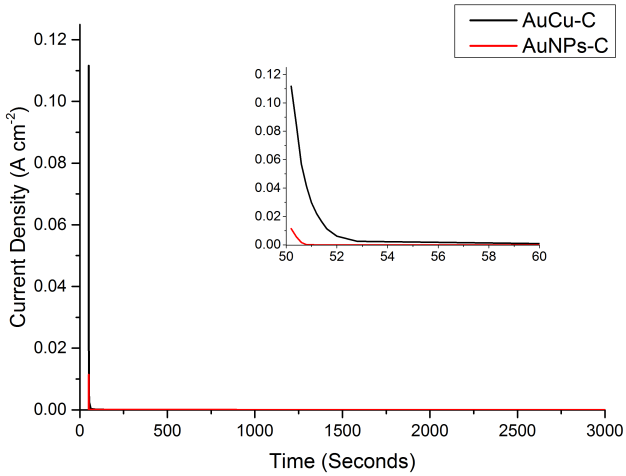

Figure.6 Chronoamperometry experiment at 0.6 V of AuCu-C and AuNPs-C catalysts in 0.5 M HCOOH + 0.5 M H_2SO_4 solution

4 Conclusion

It is clear that catalysts featuring nanometer-sized gold particles can play an important role in advancing green oxidations. AuCu-C catalysts prepared by PVP stabilized two-step reduction formed a core-shell structure with average particle size of 1.4 ± 0.11 nm. XRD evidently demonstrated the absence of superlattice and splitting reflections formation of topical to alloys and all diffraction planes shifted to lower angles confirmed AuCu core-shell structure. Cyclic voltammetry shows that AuCu-C have superior catalytic activity for formic acid oxidation when compared with commercial AuNPs dispersed on carbon black. The enhanced electrochemical activity may be due to the formation core-shell structure, which results in increased coordination unsaturated Au and Cu for small molecule hydrocarbons. Also the Cu content improved the absorption strength between active sites and the adsorbate on the catalysts. The use of PVP stabilizer showed effective coverage of Cu nanoparticles, which aid in anchorage of the Au shell on the Cu-PVP. It is reasonable to conclude that Au would reduce preferentially and cover the PVP protected Cu particles rather then on carbon because of the stronger metal interaction. The fact that Au covered Cu can be supported with XRD, CV, SEM and TEM results. These findings can provide useful guidance for turnable design protocol for HCOOH oxidation in acid solution.

Acknowledgements

The authors gratefully acknowledge funding support from Petroleum Technology Development Fund (PTDF) Scholarship of Nigeria, the University of Port Harcourt, Nigeria and the 4CU Grant EP/K001329/1. Finally, the authors would like to thank Dr. Anthony J. R. Rennie and Vitor L. Martins of the Department of Chemical & Biological Engineering, University of Sheffield, UK.

References

[1] Rees NV, Compton RG. Sustainable energy: a review of formic acid electrochemical fuel cells. Journal of Solid State Electrochemistry. 2011;15:2095-100.
[2] Evans A, Strezov V, Evans TJ. Assessment of utility energy storage options for increased renewable energy penetration. Renewable and Sustainable Energy Reviews. 2012;16:4141-7.
[3] Hadjipaschalis I, Poullikkas A, Efthimiou V. Overview of current and future energy storage technologies for electric power applications. Renewable and Sustainable Energy Reviews. 2009;13:1513-22.
[4] Rahman F, Rehman S, Abdul-Majeed MA. Overview of energy storage systems for storing electricity from renewable energy sources in Saudi Arabia. Renewable and Sustainable Energy Reviews. 2012;16:274-83.
[5] Sedighizadeh M, Rezazadeh A. Comparison between Batteries and Fuel Cells for Photovoltaic System Backup. World Academy of Science, Engineering and Technology. 2007;1:277-81.
[6] Bruni G, Cordiner S, Mulone V, Giordani A, Savino M, Tomarchio G, et al. Fuel cell based power systems to supply power to Telecom Stations. International Journal of Hydrogen Energy. 2014;39:21767-77.
[7] Carton JG, Olabi AG. Representative model and flow characteristics of open pore cellular foam and potential use in proton exchange membrane fuel cells. International Journal of Hydrogen Energy. 2015;40:5726-38.
[8] Cordiner S, Lanzani SP, Mulone V. 3D effects of water-saturation distribution on polymeric electrolyte fuel cell (PEFC) performance. International Journal of Hydrogen Energy. 2011;36:10366-75.
[9] Freedonia. World Fuel Cells
Industry Study with Forecasts for 2017 & 2022. Cleveland2014.
[10] Zhang S, Shao Y, Yin G, Lin Y. Recent progress in nanostructured electrocatalysts for PEM fuel cells. Journal of Materials Chemistry A. 2013;1:4631.
[11] Andújar JM, Segura F. Fuel cells: History and updating. A walk along two centuries. Renewable and Sustainable Energy Reviews. 2009;13:2309-22.
[12] Aslam NM, Masdar MS, Kamarudin SK, Daud WRW. Overview on Direct Formic Acid Fuel Cells (DFAFCs) as an Energy Sources. APCBEE Procedia. 2012;3:33-9.

[13] Rice C, Ha S, Masel RI, Waszczuk P, Wieckowski A, Barnard T. Direct formic acid fuel cells. Journal of Power Sources. 2002;111:83-9.
[14] An H, Cui H, Zhou D, Tao D, Li B, Zhai J, et al. Synthesis and performance of Pd/SnO2–TiO2/MWCNT catalysts for direct formic acid fuel cell application. Electrochimica Acta. 2013;92:176-82.
[15] Ha S, Larsen R, Masel RI. Performance characterization of Pd/C nanocatalyst for direct formic acid fuel cells. Journal of Power Sources. 2005;144:28-34.
[16] Rice C. Catalysts for direct formic acid fuel cells. Journal of Power Sources. 2003;115:229-35.
[17] Yu X, Pickup PG. Recent advances in direct formic acid fuel cells (DFAFC). Journal of Power Sources. 2008;182:124-32.
[18] Zhu Y, Ha SY, Masel RI. High power density direct formic acid fuel cells. Journal of Power Sources. 2004;130:8-14.
[19] Bi QY, Du XL, Liu YM, Cao Y, He HY, Fan KN. Efficient subnanometric gold-catalyzed hydrogen generation via formic acid decomposition under ambient conditions. Journal of the American Chemical Society. 2012;134:8926-33.
[20] Hu C, Pulleri JK, Ting S-W, Chan K-Y. Activity of Pd/C for hydrogen generation in aqueous formic acid solution. International Journal of Hydrogen Energy. 2014;39:381-90.
[21] Choi HJ, Kim J, Kwon Y, Han J. Comparative study of three different catalyst coating methods for direct methanol fuel cells. Journal of Power Sources. 2010;195:160-4.
[22] Baik SM, Han J, Kim J, Kwon Y. Effect of deactivation and reactivation of palladium anode catalyst on performance of direct formic acid fuel cell (DFAFC). International Journal of Hydrogen Energy. 2011;36:14719-24.
[23] Bauskar AS, Rice CA. Impact of anode catalyst layer porosity on the performance of a direct formic acid fuel cell. Electrochimica Acta. 2012;62:36-41.
[24] Oko DN, Zhang J, Garbarino S, Chaker M, Ma D, Tavares AC, et al. Formic acid electro-oxidation at PtAu alloyed nanoparticles synthesized by pulsed laser ablation in liquids. Journal of Power Sources. 2014;248:273-82.
[25] Shi M, Liu W, Zhao D, Chu Y, Ma Ca. Synthesis of palladium nanoparticles supported on reduced graphene oxide-tungsten carbide composite and the investigation of its performance for electrooxidation of formic acid. Journal of Solid State Electrochemistry. 2014;18:1923-32.
[26] Wang Z-L, Ping Y, Yan J-M, Wang H-L, Jiang Q. Hydrogen generation from formic acid decomposition at room temperature using a NiAuPd alloy nanocatalyst. International Journal of Hydrogen Energy. 2014;39:4850-6.
[27] Huang J ZZ, Yang Song, Xiongwu Kang, Ke Liu, Wancheng Zhou, Shaowei Chen. Electrocatalytic Activity of Palladium Nanocatalysts Supported on Carbon Nanoparticles in Formic Acid Oxidation. Journal of electochemistry. 2012;18:508-14.
[28] Feng L, Yao S, Zhao X, Yan L, Liu C, Xing W. Electrocatalytic properties of Pd/C catalyst for formic acid electrooxidation promoted by europium oxide. Journal of Power Sources. 2012;197:38-43.
[29] Kwon Y, Lai SCS, Rodriguez P, Koper MTM. Electrocatalytic Oxidation of Alcohols on Gold in Alkaline Media: Base or Gold Catalysis? Journal of the American Chemical Society. 2011;133:6914-7.
[30] Lee JK, Lee J, Han J, Lim TH, Sung YE, Tak Y. Influence of Au contents of AuPt anode catalyst on the performance of direct formic acid fuel cell. Electrochimica Acta. 2008;53:3474-8.
[31] Sardar R, Funston AM, Mulvaney P, Murray RW. Gold Nanoparticles: Past, Present, and Future. Langmuir. 2009;25:13840-51.
[32] Chandra P, Singh J, Singh A, Srivastava A, Goyal RN, Shim YB. Gold Nanoparticles and Nanocomposites in Clinical Diagnostics Using Electrochemical Methods. Journal of Nanoparticles. 2013;2013:12.
[33] Redina EA, Greish AA, Mishin IV, Kapustin GI, Tkachenko OP, Kirichenko OA, et al. Selective oxidation of ethanol to acetaldehyde over Au–Cu catalysts prepared by a redox method. Catalysis Today. 2015;241, Part B:246-54.

[34] Bauer JC, Mullins D, Li M, Wu Z, Payzant EA, Overbury SH, et al. Synthesis of silica supported AuCu nanoparticle catalysts and the effects of pretreatment conditions for the CO oxidation reaction. Phys Chem Chem Phys. 2011;13:2571-81.
[35] Yu X, Pickup PG. Codeposited PtSb/C catalysts for direct formic acid fuel cells. Journal of Power Sources. 2011;196:7951-6.
[36] Haruta M. Size- and support-dependency in the catalysis of gold. Catalysis Today. 1997;36:153-66.
[37] Zhu W, Michalsky R, Metin Ö, Lv H, Guo S, Wright CJ, et al. Monodisperse Au Nanoparticles for Selective Electrocatalytic Reduction of CO2 to CO. Journal of the American Chemical Society. 2013;135:16833-6.
[38] Zhu Y, Jin R, Sun Y. Atomically Monodisperse Gold Nanoclusters Catalysts with Precise Core-Shell Structure. Catalysts. 2011;1:3-17.
[39] Duan D, Liang J, Liu H, You X, Wei H, Wei G, et al. The effective carbon supported core–shell structure of Ni@Au catalysts for electro-oxidation of borohydride. International Journal of Hydrogen Energy. 2015;40:488-500.
[40] Wang G, Xiao L, Huang B, Ren Z, Tang X, Zhuang L, et al. AuCu intermetallic nanoparticles: surfactant-free synthesis and novel electrochemistry. Journal of Materials Chemistry. 2012;22:15769-74.
[41] Long NV, Hien TD, Asaka T, Ohtaki M, Nogami M. Synthesis and characterization of Pt–Pd nanoparticles with core-shell morphology: Nucleation and overgrowth of the Pd shells on the as-prepared and defined Pt seeds. Journal of Alloys and Compounds. 2011;509:7702-9.
[42] Hsu C, Wei M, Wei Z, Liu F. Improving the catalytic activity of Au/Pd core-shell nanoparticles with a tailored Pd structure for formic acid oxidation reaction. RSC Advances. 2016;6:24645-50.
[43] Villa A, Wang D, Su DS, Prati L. New challenges in gold catalysis: bimetallic systems. Catalysis Science & Technology. 2015;5:55-68.
[44] Ren M, Zhou Y, Tao F, Zou Z, Akins DL, Yang H. Controllable Modification of the Electronic Structure of Carbon-Supported Core–Shell Cu@Pd Catalysts for Formic Acid Oxidation. The Journal of Physical Chemistry C. 2014;118:12669-75.
[45] Chen CH, Liou WJ, Lin HM, Wu SH, Mikolajczuk A, Stobinski L, et al. Carbon nanotube-supported bimetallic palladium-gold electrocatalysts for electro-oxidation of formic acid. Physica Status Solidi (A) Applications and Materials Science. 2010;207:1160-5.
[46] Liu Z, Hong L, Tham MP, Lim TH, Jiang H. Nanostructured Pt/C and Pd/C catalysts for direct formic acid fuel cells. Journal of Power Sources. 2006;161:831-5.
[47] Xu JB, Zhao TS, Liang ZX. Carbon supported platinum–gold alloy catalyst for direct formic acid fuel cells. Journal of Power Sources. 2008;185:857-61.
[48] Rezaei M, Tabaian S, Haghshenas D. The Role of Electrodeposited Pd Catalyst Loading on the Mechanisms of Formic Acid Electro-Oxidation. Electrocatalysis. 2014;5:193-203.
[49] Diculescu VC, Chiorcea-Paquim A-M, Corduneanu O, Oliveira-Brett AM. Palladium nanoparticles and nanowires deposited electrochemically: AFM and electrochemical characterization. Journal of Solid State Electrochemistry. 2007;11:887-98.
[50] Ju W, Valiollahi R, Ojani R, Schneider O, Stimming U. The Electrooxidation of Formic Acid on Pd Nanoparticles: an Investigation of Size-Dependent Performance. Electrocatalysis. 2015;7:149-58.
[51] Hu S, Scudiero L, Ha S. Electronic effect on oxidation of formic acid on supported Pd-Cu bimetallic surface. Electrochimica Acta. 2012;83:354-8.
[52] Elena Soriano JM-C. Computational Mechanisms of Au and Pt Catalyzed Reactions. London: Springer; 2011.
[53] Wang X, Sun S, Huang Z, Zhang H, Zhang S. Preparation and catalytic activity of PVP-protected Au/Ni bimetallic nanoparticles for hydrogen generation from hydrolysis of basic NaBH4 solution. International Journal of Hydrogen Energy. 2014;39:905-16.